*Acta Cryst.* (1960). **13**, 516

# New Measurements of the Elastic Constants of *ADP*, and Their Relation to the Theories of Crystal Elasticity

By N. Joel and W. A. Wooster

*Crystallographic Laboratory, Cavendish Laboratory, Cambridge, England*

(*Received* 28 *October* 1959)

Some of the adiabatic elastic constants of *ADP* have been remeasured by means of Bergmann–Schaefer elastograms. The chief aim was to obtain the best possible value of the ratio $c_{44}/c_{55}$ in order to establish whether *ADP* agreed or not with the classical theory of crystal elasticity. The elastograms were measured not only along two principal axes and along the 45° direction, as has been customary so far, but also in many directions in the same plane. These measurements were used for determining the $c_{ij}$ by means of least-squares methods. The results are:

$$c_{11}=66{\cdot}9,\ \ c_{33}=32{\cdot}8,\ \ c_{13}=19{\cdot}9,\ \ c_{44}=8{\cdot}8,\ \ c_{55}=8{\cdot}3\ (0{\cdot}10^{10}\text{ dyne cm.}^{-2}).$$

The ratio $c_{44}/c_{55}$ is $1{\cdot}06\pm0{\cdot}02$, thus confirming the validity of Laval's contention that 21 elastic constants are not in general sufficient for describing the elastic properties of crystals.

## 1. Introduction

Laval's work (1951, 1952, 1957) indicated that the number of elastic constants required to describe the elastic properties of a crystal is greater than the number required by the classical theory of Voigt and the lattice theory of Born & Huang (1954). This was first tested experimentally by LeCorre (1954) who made a determination of the elastic constants of *ADP*, class $\bar{4}2m$, and found a difference of 36% between two elastic constants which are equal on Voigt's formulation:

$$c_{44}=10{\cdot}3\pm0{\cdot}6,\ \ c_{55}=7{\cdot}6\pm0{\cdot}5\ (0{\cdot}10^{10}\text{ dyne cm.}^{-2})\ .$$

Zubov & Firsova (1956) remeasured the elastic constants of quartz and found differences of just over 1% and 3% respectively where the classical theory demanded none:

$$c_{44}=58{\cdot}5,\ c_{55}=57{\cdot}7\ ;\ \ c_{14}=18{\cdot}3,\ c_{17}=17{\cdot}7\ .$$

Both these determinations were made by means of Bergmann–Schaefer elastograms. In those cases where it can be used this seems to be the best method of obtaining good relative values for the elastic constants.

We made attempts to determine which of the 32 crystal classes are more likely to show any departures from the classical formulation. We showed (Joel & Wooster, 1958*a*) that, on the basis of a fundamental principle, the number of independent elastic constants reduces in the general case from Laval's 45 to 39. There appears to be no difference between the old and the new theories for isotropic solids and for the cubic classes 432, $\bar{4}3m$, $m3m$. The assumption on which these results were obtained was either:

(*a*) rotations of undeformed elements of volume do not contribute to the strain energy; that is, the strain energy of a crystal is invariant under rotations of undeformed elements of volume, or

(*b*) body couples can arise in a given element of volume subjected to strain only if this strain is more than a simple rotation of the volume element.

One of the consequences of the new approach, with its increased elastic matrices, is that body-couples may be acting in a deformed element of volume to balance the non-symmetric stress tensor. It is possible that, if consideration is given to the mechanism responsible for the appearance of these body-couples, some further restrictions may arise on the number of independent elastic constants, or on the crystal classes affected by the new theory. For instance, a tentative hypothesis (made plausible by the structural features of those crystals which have so far shown departures from the classical theory) could be that helicoidal features in the crystal structure might be the responsible mechanism (Joel & Wooster, 1957). This would lead to the result that, through symmetry requirements, the effects would cancel out in all crystal classes except the 11 enantiomorphous ones and the four classes: $m$, $mm$, $\bar{4}$ and $\bar{4}2m$. These 15 classes are the same as those which can show optical activity. Thus there would be only 14 classes available for testing the new theory, as the enantiomorphous class 432 is excluded on the more general principle given above.

The only crystals belonging to any of these 14 classes that we know to have been studied by the Bergmann–Schaefer method are: quartz (32), *ADP* and *KDP* ($\bar{4}2m$), sodium chlorate (23) and Rochelle salt (222). And there are not many more that lend themselves to study by this method. Quartz was studied by Nomoto (1943), *ADP* and *KDP* by Zwicker (1946), sodium chlorate and Rochelle salt by Jona

(1950), all of them before the publication of Laval's work, and at a time when any small discrepancies between certain elastic constants expected to be equal would have been attributed to experimental errors.

Then came the work of LeCorre (1954) and of Zubov & Firsova (1956) mentioned above, on *ADP* and quartz respectively. They did find a departure from Voigt's formulation. But the difference found by LeCorre between $c_{44}$ and $c_{55}$ (quoted above) seems rather large to have escaped Zwicker's attention in 1946. Therefore it was considered of interest to redetermine the elastic constants of *ADP* by means of Bergmann–Schaefer elastograms, with special emphasis on the ratio $c_{44}/c_{55}$. This interest was increased by the fact that on carefully remeasuring Zwicker's *YZ** elastogram of *ADP*, a difference of about 8% was found between $c_{44}$ and $c_{55}$ (Joel & Wooster, 1958*b*; in this paper some details are also given on the generation, interpretation and calculation of the elastograms which need not be repeated here.)

## 2. Apparatus

The general principles of the method are well known (Bergmann, 1954). Only such details as are required by the description of our apparatus will be given here.

The electronic equipment consists of two parts:

(i) A power supply which is fed from the mains (200 V. a.c., 50 Hz.) and delivers 800 V. d.c. to the oscillator.

(ii) The oscillator, which is shown diagrammatically in Fig. 1. The characteristics of its resonant circuit are such that if a negligible capacitance is placed between the two output terminals, the frequency range is from 5·5 to 9·8 mHz. But with the quartz plate in place these frequencies become smaller, and in our work we used a range from about 4·8 to 7·0 mHz. The power output of the oscillator can be regulated in four steps, and under working conditions the mA.-meter (Fig. 1) reads between 100 and 200 mA.

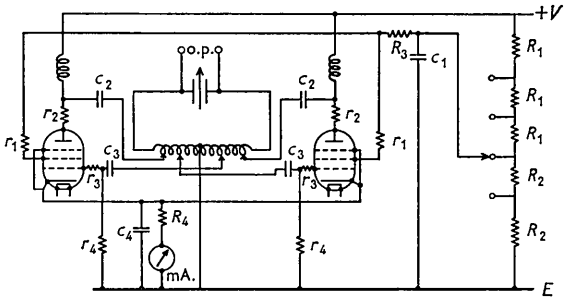


Fig. 1. Circuit diagram of the oscillator $R_1$ 5 kΩ W.W.; $R_2$ 10 kΩ W.W.; $R_3$ 750 Ω W.W.; $R_4$ 100 Ω W.W.; $r_1$ 47 Ω; $r_2$ 12 Ω; $r_3$ 120 Ω; $r_4$ 150k Ω; $C_1$ 8 μF.; $C_2$ 600 pF. (15 kV.); $C_3$ 22 pF.; $C_4$ 0·1 μF.; mA. 0–250 mA.; valves EL 34 V. 800 v.

The frequency of the elastic waves for every elastogram was measured first, approximately, by means of an absorption wave meter (accuracy about 1%), and then with a frequency meter of the beat frequency type, model BC. 221-M made by Bendix Radio (accuracy better than 0·01%).

For the purpose of observing the diffraction patterns, we found it a great advantage to use the 'optical diffractometer' the main characteristics of which are shown in Fig. 2(*a*). A more detailed description of a similar instrument can be found in a paper by Hughes & Taylor (1953).

The source of light *S* is a 250 W. mercury vapour lamp type *ME/D*, (Mazda); by means of a filter the orange line of the mercury spectrum ($\lambda = 5780$ Å) was selected. The diameter of the pinhole *P* is of the order of 0·02 mm., but in our experiments the spots in the focal plane *F* of the objective lens *L'* are larger, of the order of 0·05 mm., due to the diffraction introduced by the limited cross section of the crystal. Both lenses *L* and *L'* have a long focal length (about 130 cm. in this instrument): the longer the focal length of *L*, the better the resolution; and the longer the focal length of *L'*, the larger the size of the diffraction pattern at *F*. Our elastograms measure about 3 to 4 mm. across.

The main advantage of this design of the diffractometer is that the mirror *M* makes it possible to manipulate the crystal *C* Fig. 2(*b*) and the iris diaphragm *D* while looking through the eyepiece *E* at the elastogram

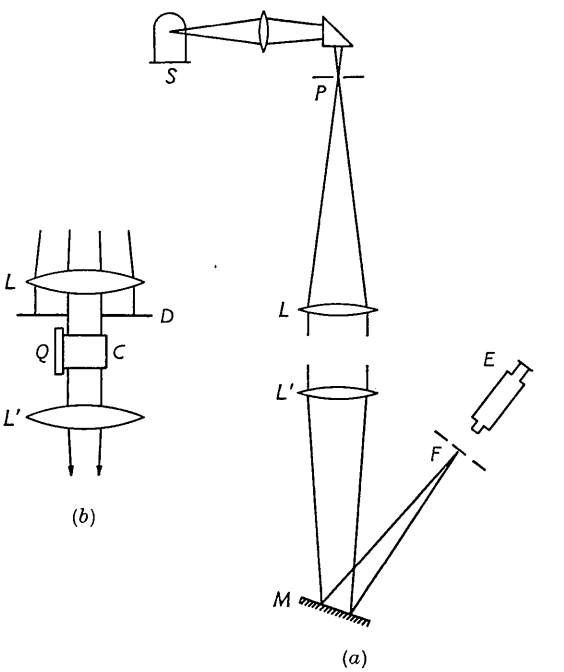


Fig. 2. (*a*) The optical diffractometer. (*b*) Arrangement of the crystal *C* on the oscillating quartz plate *Q*.

* Crystallographers normally use *X*, *Y*, *Z* to denote crystallographic axes whereas in work involving tensors the axes are denoted $X_1$, $X_2$, $X_3$. No attempt is made here to avoid using both systems.

located at $F$. This facilitates the setting of the diaphragm relative to the crystal. It is necessary to keep out all stray light, select the largest possible diameter that will give a good image, and avoid regions of poor optical quality in the crystal should they exist. When the crystal and diaphragm are in position, it is possible to adjust the frequency of the oscillator (by means of its variable condenser) until the best elastogram can be seen through the eyepiece.

If the crystal under investigation is itself piezoelectric, it can be excited directly, without attaching a quartz plate to it. But, because the intensity distribution on the elastograms is more uniform when the elastic waves in the crystal originate from an attached quartz plate, we used this indirect excitation of the crystal throughout our work. We have used several sizes of quartz plates; the best results were obtained with one of area a little larger than that of the contact surface and of thickness about 5 mm. The plates were cut perpendicular to the $X$ axis, and thin coatings of gold or silver formed the electrodes. The thickness of these electrodes is such that the resistance of one of them, measured from one end of the plate to the other, is of the order of 1 Ohm.

It was found that the quartz plate was best attached to the crystal by means of a thin layer of the silicon grease used in vacuum work. Slight pressure and a little to-and-fro sliding motion of the crystal on the quartz plate ensures good contact, provided that both surfaces are sufficiently flat. The quality of the contact can be checked by looking obliquely at the contact surface through the crystal.

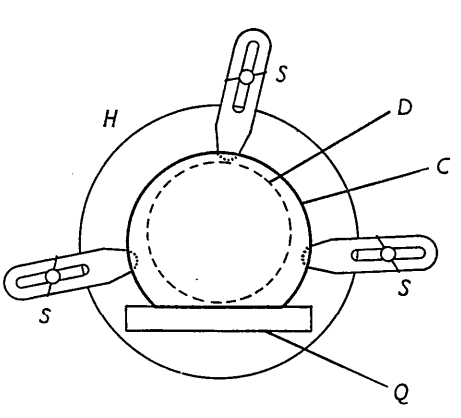


Fig. 3. Diagram of the arrangement for supporting the crystal, $C$: $P$, base plate, $S$, screws clamping the arms which support the crystal; $H$, aperture in $P$; $D$, iris diaphragm; $Q$, the quartz oscillator.

The crystal rests on the ends of three small flat-topped rods that can slide on the plate $P$ (Fig. 3) and can be kept in position by means of the screws $S$. In this way, specimens of different sizes and shapes can be used. A circular hole $H$ in the plate $P$ allows the passage of the light, and on $P$ rests a holder for the iris diaphragm $D$.

The elastogram formed at $F$ (Fig. 2($a$)) can be photographed by placing in its plane a photographic plate or film. We found it convenient to use a film holder (with a shutter) which could be attached to the microscope and which took short strips of 35 mm. film capable of recording 4 or 5 successive elastograms. The film used was Ilford *HP*3. The faster film, *HPS*, was also tried, but it did not prove to be more useful than the *HP*3 because it showed a more intense background due to stray light.

### 3. The specimen of *ADP*

The specimens must have two flat, optically polished, parallel faces through which the light enters and leaves the crystal, and also a flat face, perpendicular to the other two, to which the driving quartz plate is attached. The shape of the specimen can have an important effect on the intensity, though not on the position, of the spots in the elastogram. This is due to the reflection of the elastic waves on the lateral surface of the specimen, which is in contact with the air. The acoustic impedance of *ADP* for its longitudinal waves is of the order of $10^6$ c.g.s. units, while that of the air surrounding it is about 40 c.g.s. units. Therefore, total reflection occurs (reflectivity at normal incidence, under these circumstances, differs from unity by only $10^{-4}$). The reflected waves are not only longitudinal but also transverse, and it is precisely these transverse waves, particularly those travelling along the axes $Y$ and $Z$, which are required for the present work. On the elastograms, the inner curve is caused by diffraction at the longitudinal elastic waves, and the outer curve (or curves) by diffraction at the transverse (shear) waves.

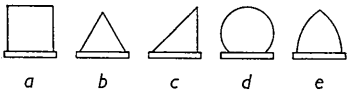


Fig. 4. Shapes of optical glass which were tested for the influence of the geometrical form on the diffraction pattern.

The best elastograms are obtained when elastic waves travel in all directions within the plane perpendicular to the direction of travel of the light. To achieve this, the lateral surface of the specimen (on which the longitudinal waves coming from the quartz plate are reflected) must be a curved surface generated by straight lines perpendicular to the two parallel end faces of the specimen. In order to find the best shape we tried specimens of optical glass of different cross sections, as shown in Fig. 4. Specimen ($a$) gives very strong spots corresponding to the longitudinal elastic waves travelling in directions parallel to the sides of the square, and very little of the elastic energy goes into transverse waves. Specimens ($b$) and ($c$) were tried in order to compare the reflections at the inclined faces with the theoretical predictions. Their elastograms show very prominently the spots

due to the waves reflected from the side faces (both longitudinal and transverse), and if more power is put in then more spots appear. But the elastograms are not uniform but rather 'spotty'. Specimens (*d*) and (*e*) give good continuous elastograms, particularly (*d*). Spangenberg & Haussühl (1957) and Haussühl (1957) recommend the 'gothic arch' (*e*), but under the conditions of our experiments we found that the cylinder (*d*) gave better results.

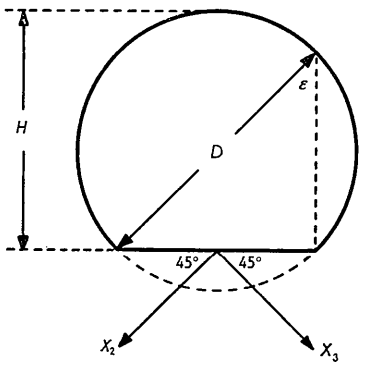


Fig. 5. Diagram of the shape, size and orientation of the specimen of *ADP*. $H=32$ mm., $D=36$ mm.

A specimen of *ADP* was ground to the shape (*d*), with the crystallographic orientation shown in Fig. 5: the cross section is the plane *YZ*, which is the setting required for the determination of the ratio $c_{44}/c_{55}$. With this orientation, the waves that contribute to the two curves of the elastogram are quasi-longitudinal and quasi-transverse respectively, and their amplitude vectors (vibration directions) are parallel to the plane *YZ*. The axes *Y* and *Z*, in the plane of the cross section, are both at 45° to the flat surface in contact with the quartz plate. This orientation of the axes *Y* and *Z* was chosen because it can give rise to shear waves travelling along *Y* and *Z*.

As even the elastogram of this cylindrical specimen did not show the regions that are most important for this work—namely the portions of the outer curve near the *Y* and *Z* axes—specimens of the shape and orientation shown in Figs. 6 and 7 were made. These should show prominently the points $T_y$ and $T_z$ at which the outer curve of the elastogram intersects the *Y* and *Z* axes.* Neither of these specimens gave the points $T_y$ and $T_z$ in spite of the existence of the corresponding elastic waves along *Y* and *Z*. This behaviour of both the cylindrical and the two prismatic specimens can only be attributed to the elasto-optical properties of the crystal. Besides, the elastograms of the two prismatic specimens were not at all uniform and rather spotty, as could be expected.

The work described below was therefore carried out on the cylindrical specimen (Fig. 5) which, even if it does not show the spots $T_y$ and $T_z$, is the one that gave the most complete and uniform elastograms. Its dimensions are: $D=36$ mm., $H=32$ mm., which give for the longitudinal waves incident on the curved surface a variable angle of incidence $\varepsilon$ ranging from 0° to about 40°. ($\varepsilon \sim 32°$ is the angle of incidence required for the reflected shear waves to travel along *Y* and *Z*.) The height of the cylinder, parallel to the direction of travel of the light, is 25 mm., and the axes *Y* and *Z* are disposed symmetrically to the flat side-face. The dimensions of this specimen would permit the observations to be carried out with a circular diaphragm of diameter up to about 30 mm. In fact, the homogeneity of the crystal and the quality of the optical polish were so good that a diaphragm as large as 25 mm. could actually be used, giving very good resolution. The two optically polished faces were parallel to each other within less than 1′ of arc; their orientation relative to the crystal lattice was checked by means of X-ray diffraction and found to be correct, that is, parallel to the planes (100), within less than 10′ of arc; the axes *Y* and *Z* were in their 45° direction within less than 15′ of arc, but this is not an essential point because the measurements on the elastogram can be made independently. The only important requirement is that the two parallel end faces of the crystal should be parallel to *YZ* and perpendicular to the direction of travel of the light. This last condition, the setting of the crystal on the diffractometer, was checked by means of an inclinometer (precision spirit level provided with a micrometer screw) which is accurate to 30″ of arc. It was possible

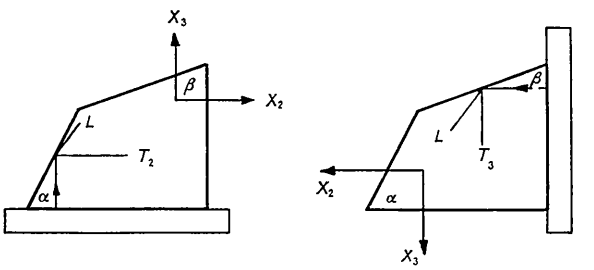


Fig. 6.

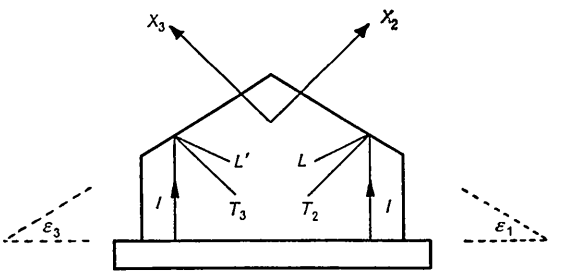


Fig. 7.

Figs. 6 & 7. Diagrams of shapes of crystal chosen to accentuate spots corresponding to transverse waves $T_2$, $T_3$, travelling along axes $X_2$ and $X_3$ respectively.

* Details of the calculations that lead to the appropriate angles in these specimens together with other relations between the elastograms and the reflected waves will be given elsewhere.

to keep the crystal in its correct orientation within less than 5′ of arc.

So, the accuracy of the orientation of the specimen in the beam of light is well within the experimental requirements. A quantitative discussion of the errors is given in Section 6, after the results.

## 4. Recording of the elastograms

Two of the elastograms recorded with the cylindrical specimen are shown in Fig. 8(*a*), (*b*): (*a*) with a short exposure time, 1 sec.; (*b*) with a longer exposure time, 30 sec. The latter was made in six parts of 5 sec. each, with 5 min. interval between consecutive exposures. This was done because, under the conditions of our work, after more than about 8 sec. the image began to deteriorate owing to inhomogeneous heating of the crystal: a temperature gradient was formed, with the warmer end next to the quartz plate. It was also noticed that this effect was considerably greater on the ordinary than on the extraordinary beam of light; this could be checked quite simply by rotating a polaroid placed between the microscope eyepiece and the eye. Therefore a good quality polaroid was placed near the image plane just below $F$ (Fig. 2(*a*)) in a position such that it only transmitted the light with amplitude vector parallel to the $Z$ axis of the crystal. This caused an increase in the exposure time by a factor of more than 2, but it also improved the resolution.

## 5. Interpretation of the elastograms

In a medium with adiabatic elastic stiffnesses $c_{\alpha\beta\gamma\delta}$, the velocities, $v$, of the three elastic waves with wave-normals parallel to the unit vector $\mathbf{q}(q_1, q_2, q_3)$ are given by:

$$\begin{vmatrix} A_{11}-Q & A_{12} & A_{13} \\ A_{12} & A_{22}-Q & A_{23} \\ A_{13} & A_{23} & A_{33}-Q \end{vmatrix} = 0 \qquad (1)$$

where:

$A_{\alpha\gamma} = \sum_{\beta\delta} c_{\alpha\beta\gamma\delta} q_\beta q_\delta \qquad (\alpha, \beta, \gamma, \delta = 1, 2, 3),$

$\varrho$ is the density of the crystal,

$Q = \varrho v^2$ is the elastic stiffness for each of the three waves.

The directions of the amplitude vectors $\mathbf{u}$ of the three waves, that is, their vibration directions, are given by the set of three linear equations:

$$\left.\begin{aligned} (A_{11}-Q)u_1 + A_{12}u_2 + A_{13}u_3 &= 0 \\ A_{12}u_1 + (A_{22}-Q)u_2 + A_{23}u_3 &= 0 \\ A_{13}u_1 + A_{23}u_2 + (A_{33}-Q)u_3 &= 0 \end{aligned}\right\} \qquad (2)$$

where $Q$ has to be given in turn the value of each of the three roots of equation (1).

The elastic matrix of *ADP* has 9 independent components in the Laval theory. But, as mentioned in Section 1, we have shown that they are not all independent. There are two relations between Laval's constants for *ADP*:

$$c_{47} = \tfrac{1}{2}(c_{44} + c_{55}) \qquad (3)$$

$$c_{69} = c_{66} \, . \qquad (4)$$

The elastic matrix becomes:

$$\left.\begin{array}{cccccccccc} 11 & 12 & 13 & . & . & . & . & . & . \\ 12 & 11 & 13 & . & . & . & . & . & . \\ 13 & 13 & 33 & . & . & . & . & . & . \\ . & . & . & 44 & . & . & 47 & . & . \\ . & . & . & . & 55 & . & . & 47 & . \\ . & . & . & . & . & 66 & . & . & 66 \\ . & . & . & 47 & . & . & 55 & . & . \\ . & . & . & . & 47 & . & . & 44 & . \\ . & . & . & . & . & 66 & . & . & 66 \end{array}\right\} \qquad (5)$$

where the relation (3) involving $c_{47}$ has to be kept in mind.

The wave-normals are restricted to the $YZ$ plane, so that $q_1 = 0$. Let us substitute $q_2 = m = \cos\varphi$, $q_3 = n = \sin\varphi$, where $\varphi$ is the angle between the wave-normal and the $Y$ axis. Thus the $A_{\alpha\gamma}$ become:

$$\left.\begin{aligned} A_{11} &= c_{66}m^2 + c_{44}n^2 = c_{44} + (c_{66} - c_{44}) \cos^2\varphi \\ A_{22} &= c_{11}m^2 + c_{44}n^2 = c_{44} + (c_{11} - c_{44}) \cos^2\varphi \\ A_{33} &= c_{55}m^2 + c_{33}n^2 = c_{33} - (c_{33} - c_{55}) \cos^2\varphi \\ A_{23} &= (c_{13} + c_{47})mn = \tfrac{1}{2}(c_{13} + c_{47}) \sin 2\varphi \\ A_{12} &= A_{13} = 0 \, . \end{aligned}\right\} \qquad (6)$$

In view of the relation (3) and the expression for $A_{23}$ in (6), it will be convenient to introduce:

$$c = c_{13} + \tfrac{1}{2}(c_{44} + c_{55}) \, . \qquad (7)$$

The elastic waves have the frequency $\nu$ imposed by the oscillator, and therefore their wave-length $\Lambda$ is:

$$\Lambda = v/\nu = (Q/\varrho)^{\frac{1}{2}}/\nu. \qquad (8)$$

The elastic wave-fronts give rise to Bragg reflexions and the Bragg angle $\theta$ is given by the relation

$$2\Lambda \sin\theta = \lambda \, . \qquad (9)$$

The angle $\theta$ is of the order of a few minutes of arc only as the ratio $\lambda/\Lambda$ is of the order of $10^{-3}$. Therefore, for all practical purposes, the waves giving rise to the diffraction pattern have their wave-normals perpendicular to the optical axis of the system.

It was shown by Fues & Ludloff (1935) that the deviation $2\theta$ of any diffracted beam is independent of the refractive index of the crystal for the light being used. The refractive index on the one hand decreases the wavelength of the light in the crystal, with a proportional decrease in $\sin\theta$; but on the other hand it gives rise to refraction of the diffracted beam on leaving the crystal. For such small angles as occur in this case, the two effects compensate. It is because of this that both the ordinary and the extraordinary vibrations give rise to the same diffraction patterns.

If the lens $L'$ (Fig. 1) has a focal length $f$, the cor-

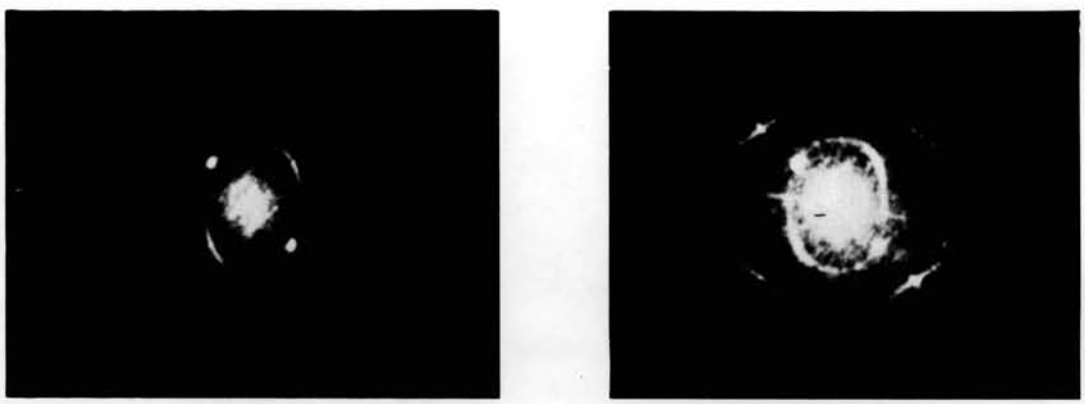

(*a*) (*b*)

Fig. 8. Elastograms of *ADP* at $\nu = 4980{\cdot}8$ kc.
(*a*) exposure time 1 sec. (*b*) exposure time six intervals of 5 sec. each.

[*To face p. 520*

responding separation $r$ between the image of the pinhole and the diffracted spot is:

$$r=2\theta f=\lambda f/\Lambda=\lambda f\nu/v=\lambda f\nu(\varrho/Q)^{\frac{1}{2}}. \quad (10)$$

From this formula it follows that if on an elastogram the diametral distance $2r$ between symmetrically opposed spots is measured, the elastic stiffness $Q$ is:

$$Q=\lambda^2 f^2\nu^2\varrho/r^2. \quad (11)$$

It can be seen that for the relative values of the elastic constants that can be obtained from one elastogram, the only errors involved are those occurring in the measurements of $2r$, ($\Delta Q/Q=-2\Delta r/r$). If different elastograms, taken with different frequencies, have to be compared, the only additional error which must be considered is that in $\nu$. The frequency $\nu$ was measured with an accuracy better than 0·01%, and therefore it can be said that the accuracy of our ratio $c_{44}/c_{55}$ and, in general, of the relative values of $Q$, depends only on the accuracy of the measurements of $2r$. For this reason this method is the most suitable for the purpose of obtaining the best possible value for the ratio $c_{44}/c_{55}$.

In the course of the work, several elastograms had to be calculated and drawn, and the appropriate scale was found to be such that

$$Q=10^{13}/R^2\,. \quad (12)$$

From (11) and (12) it follows that the scale factor relating $R$ and $2r$ is:

$$R = \gamma.2r\,. \quad (13)$$

$$\gamma = (10^{13}/\varrho)^{\frac{1}{2}}/(2\lambda f\nu)\,. \quad (14)$$

$\varrho$, $\lambda$ and $f$ are constant throughout this work; their numerical values are:

$$\lambda = 5780\times10^{-8}\text{ cm.}$$
$$f = 132{\cdot}0\text{ cm. }(\pm0{\cdot}5\text{ cm.}).$$
$$\varrho = 1{\cdot}790\text{ g.cm.}^{-3}.$$

Hence

$$\gamma = 154{\cdot}9/\nu\times10^6. \quad (15)$$

The elastograms of Fig. 8 were taken with $\nu=(4980{\cdot}8\pm0{\cdot}2)$ kHz., so that for them:

$$\gamma=31{\cdot}10\,. \quad (16)$$

The results of the measurements of the diameters $2r_L$ and $2r_T$ in a given direction in the plane $YZ$ (Fig. 8) are used to calculate first $R_L$ and $R_T$ by means of (13) and (15), and then $Q_L$ and $Q_T$ by means of (12).

These two values of $Q$ are, according to (1) and (6), the roots of the equation

$$(A_{22}-Q)(A_{33}-Q)-A_{23}^2=0\,. \quad (17)$$

Along the $Y$ axis, $Q_L=c_{11}$ and $Q_T=c_{55}$, while along the $Z$ axis, $Q_L=c_{33}$ and $Q_T=c_{44}$. In all other directions in the plane $YZ$, $Q_L$ and $Q_T$ are functions of the 5 stiffnesses $c_{11}$, $c_{33}$, $c_{44}$, $c_{55}$ and $c$.

Measurements on the inner curve along the axes $Y$ and $Z$, therefore, provide the values of $c_{11}$ and $c_{33}$. The values of $c_{44}$ and $c_{55}$ cannot be obtained as directly as the previous ones, for the reasons already stated. But a study of the equation of the elastogram showed that it was possible to devise a good extrapolation scheme on the following lines.

Equation (17) can be written:

$$Q^2-(A_{22}+A_{33})Q+A_{22}A_{33}-A_{23}^2=0 \quad (18)$$

and it follows that:

$$Q_L+Q_T=A_{22}+A_{33}\,. \quad (19)$$

From (6) and (19), and by introducing the parameters

$$g = c_{11}+c_{55}$$
$$h = c_{33}+c_{44}\,, \quad (20)$$

it follows that

$$Q_L+Q_T=h+(g-h)\cos^2\varphi\,. \quad (21)$$

So, if $2r$ is measured in several directions for both the inner and the outer curve, and $Q_L+Q_T$ is plotted against $\cos^2\varphi$, a straight line should be obtained; and extrapolation to $\cos^2\varphi=1$ and 0 gives the values of $g$ and $h$ respectively. Instead of plotting the straight line, $g$ and $h$ can be calculated more accurately from a least-squares solution of a large set of linear equations in two variables in the following way:

Equation (21) can be written:

$$m^2g+n^2h=Q_L+Q_T\,. \quad (22)$$

Each measurement gives one set of data

$$(m^2,\ n^2,\ Q_L+Q_T)$$

and corresponds to one equation. The standard method can now easily be applied (see for instance Topping, 1955).

Having thus obtained the values of $g$ and $h$, the stiffnesses $c_{44}$ and $c_{55}$ follow then immediately from equations (20) as $c_{11}$ and $c_{33}$ have already been obtained directly. Details of these measurements and calculations will be given in Section 6.

There is another way of calculating $c_{44}$ and $c_{55}$ from our data, which does not require the previous measurement of $c_{11}$ and $c_{33}$: the five parameters of the equation of the elastogram are determined directly by means of a least-squares computation in five variables, making use of the large number of measurements for $Q_L$ and $Q_T$ in different directions. But the coupling between the stiffnesses $c_{ij}$ is such that if they are taken as variables the calculation becomes far too complicated. But a very simple way of dealing with this problem was found as follows:

Equation (18) can be written with the help of (6):

$$Q^2-[(c_{11}+c_{55})m^2+(c_{33}+c_{44})n^2]Q+c_{11}c_{55}m^4 + c_{33}c_{44}n^4+(c_{44}c_{55}+c_{11}c_{33}-c^2)m^2n^2=0 \quad (23)$$

and by substituting:

$$\left.\begin{aligned} c_{11}+c_{55}&=a_1\\ c_{33}+c_{44}&=a_2\\ c_{11}c_{55}&=a_3\\ c_{33}c_{44}&=a_4\\ c_{11}c_{33}+c_{44}c_{55}-c^2&=a_5 \end{aligned}\right\} \qquad (24)$$

equation (23) becomes:

$$m^2Qa_1+n^2Qa_2-m^4a_3-n^4a_4-m^2n^2a_5=Q^2. \qquad (25)$$

The five parameters $a_i$ can be calculated by means of a linear least-squares computation, and then the $c_{ij}$ follow from (24). Details of these calculations will be given in Section 6.

## 6. Measurements and results

The measurements were made with a travelling microscope which could be read to 0·001 mm., and in order to be able to measure $2r$ in any desired direction, the elastogram was placed on the rotatable stage of a microscope. The magnification of the spot or line was 46. To test for any effects, due to the contraction of the photographic film or to distortions caused by any part of the optical train, some measurements were performed using a glass cube as the diffracting body. Three measurements of the diameter of a ring, 2·832 mm. across, were taken along the length of the 35 mm. strip and three corresponding measurements were made across the strip. None of these six measurements differed from the mean value by as much as 0·002 mm. We may therefore take this value as the possible error in any one measurement, and any difference in the shrinkage of the film along and perpendicular to its length may be neglected.

It is necessary to ensure that the two readings used for a determination of $2r$ are actually taken at symmetrically opposed points, which require (i) that the centre of the elastogram coincides with the centre of the revolving stage, and (ii) that during the travel of the microscope, the fiducial mark used for the settings (intersection of crosswires) actually goes through the centre of the elastogram. This could be achieved with an error of just less than 0·01 mm. Then it is necessary to determine the settings of the stage that correspond to measurements along $Y$ and $Z$; this could be done by making repeated measurements around these axes until equal values were obtained for readings taken at symmetrical positions. $2r_T$ (outer curve) was measured on elastograms such as Fig. 8($b$); while $2r_L$ (inner curve) was measured mainly on elastograms such as Fig. 8($a$). In some cases, measurements of both $2r_T$ and $2r_L$ could be made on the same elastogram.

Those measurements were made first which gave $c_{11}$ and $c_{33}$ directly. Several elastograms such as Fig. 8($a$) were measured, and each elastogram was measured several times. The readings on the travelling microscope were taken 10 times and from their average a value of $Q_L$ ($c_{11}$ or $c_{33}$) was calculated. The results of twelve independent determinations made on three different elastograms give:

$$c_{33}=(32{\cdot}8\pm0{\cdot}04)\times10^{10}\text{ dyne cm.}^{-2},$$
$$c_{11}=(66{\cdot}9\pm0{\cdot}12)\times10^{10}\text{ dyne cm.}^{-2}.$$

In order to apply the '$gh$' procedure (equations (20), (21), (22)), measurements of $2r_L$ and $2r_T$ in several directions in the plane $YZ$ had now to be made. These were made in steps of 3° in $\varphi$ ($\cos\varphi=m$), Fig. 9. In each position, between six and ten readings were taken on the travelling microscope and averaged. Furthermore, the results quoted for a given value of $\varphi$ are, whenever possible, averages of results obtained in the four positions: $\varphi$, $180-\varphi$, $180+\varphi$, $360-\varphi$ (Fig. 9). On the outer curve, for any given $\varphi$, these

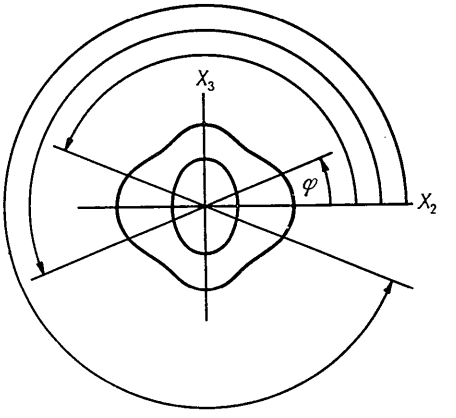


Fig. 9. The four different positions of the rotating stage at which measurements were made for a given value of $\varphi$.

four values hardly ever differed by more than 0·015 mm., usually less than 0·01 mm. Table 1 shows the results of one typical set of measurements. The corresponding graph of $Q_L+Q_T$ against $\cos^2\varphi$ is shown in Fig. 10.

As $R$ is about 30 times $2r$ (formulae 13 and 16), it follows that the uncertainty in the values of $R$ given in mm. in Table 1 is of the order of 1 unit of the first decimal figure. As the values of $2r_T$ are larger than those of $2r_L$, and also because the inner curve always happened to have some regions of poor

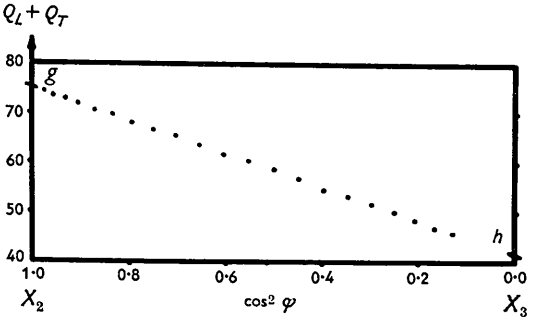


Fig. 10. $Q_L+Q_T$ plotted against $\cos^2\varphi$, Set 2.

Table 1. *Radii of longitudinal and transverse curves on the elastogram of Fig. 8, together with the corresponding calculated values of $Q_L$ and $Q_T$*

| $\varphi$ | $2r_L$ | $2r_T$ | $R_L$ | $R_T$ | $Q_L$ | $Q_T$ | $Q_L+Q_T$ | $\cos^2\varphi$ |
|---|---|---|---|---|---|---|---|---|
| 9 | 1·253 | 3·472 | 39·0 | 108·0 | $65{\cdot}7_4$ | 8·75 | 74·3 | 0·9755 |
| 12 | 1·265 | 3·438 | 39·3 | 106·9 | $64{\cdot}7_4$ | 8·75 | 73·5 | 0·9568 |
| 15 | 1·273 | 3·390 | 39·6 | 105·4 | $63{\cdot}7_7$ | 9·00 | 72·8 | 0·9330 |
| 18 | 1·288 | 3·328 | 40·0 | 103·5 | $62{\cdot}5_0$ | 9·34 | 71·8 | 0·9045 |
| 21 | 1·301 | 3·270 | 40·5 | 101·7 | $60{\cdot}9_6$ | 9·67 | 70·6 | 0·8716 |
| 24 | 1·316 | 3·211 | 40·9 | 99·9 | $59{\cdot}7_8$ | 10·02 | 69·8 | 0·8346 |
| 27 | 1·339 | 3·160 | 41·6 | 98·3 | $57{\cdot}7_8$ | 10·35 | 68·1 | 0·7939 |
| 30 | 1·360 | 3·108 | 42·3 | 96·7 | $55{\cdot}8_9$ | 10·69 | 66·6 | 0·7500 |
| 33 | 1·378 | 3·045 | 42·9 | 94·7 | $54{\cdot}3_4$ | 11·15 | 65·5 | 0·7034 |
| 36 | 1·408 | 2·990 | 43·8 | 93·0 | $52{\cdot}1_3$ | 11·56 | 63·7 | 0·6545 |
| 39 | 1·440 | 2·936 | 44·8 | 91·3 | $49{\cdot}8_2$ | 12·00 | 61·8 | 0·6040 |
| 42 | 1·463 | 2·895 | 45·5 | 90·0 | $48{\cdot}3_0$ | 12·35 | 60·6 | 0·5523 |
| 45 | 1·500 | 2·863 | 46·6 | 89·0 | $46{\cdot}0_6$ | 12·62 | 58·7 | 0·5000 |
| 48 | 1·531 | 2·850 | 47·6 | 88·6 | $44{\cdot}1_3$ | 12·74 | 56·9 | 0·4477 |
| 51 | 1·572 | 2·834 | 48·9 | 88·1 | $41{\cdot}8_2$ | 12·88 | 54·7 | 0·3960 |
| 54 | 1·598 | 2·836 | 49·7 | 88·2 | $40{\cdot}4_9$ | 12·85 | 53·3 | 0·3455 |
| 57 | 1·629 | 2·843 | 50·7 | 88·4 | $38{\cdot}9_0$ | 12·80 | 51·7 | 0·2966 |
| 60 | 1·660 | 2·867 | 51·6 | 89·2 | $37{\cdot}5_6$ | 12·57 | 50·1 | 0·2500 |
| 63 | 1·694 | 2·903 | 52·7 | 90·3 | $36{\cdot}0_1$ | 12·26 | 48·3 | 0·2061 |
| 66 | 1·720 | 2·952 | 53·5 | 91·8 | $34{\cdot}9_4$ | 11·87 | 46·8 | 0·1654 |
| 69 | 1·733 | 3·016 | 53·9 | 93·8 | $34{\cdot}4_2$ | 11·37 | 45·8 | 0·1284 |

resolution, the maximum errors $\Delta Q_T$ are smaller than the $\Delta Q_L$. In the regions of small $\varphi$, ($Q_L \sim 60$), $\Delta Q_L$ is of the order of 0·3; while for large $\varphi$, ($Q_L \sim 35$), $\Delta Q_L$ is about 0·1. On the other hand, $\Delta Q_T$ is about 0·02 to 0·03 (for $Q_T \sim 9$ to 12).

Three independent sets such as that shown in Table 1 were measured and evaluated. In each of them the elastograms were recentred and the procedure outlined above was followed. The parameters $g$ and $h$ were calculated by means of a least-squares solution of simultaneous linear equations (2 variables, 21 equations in each set). The results are, for $g$: 75·3, 75·1, 75·2; and for $h$: 41·6, 41·6, 41·5, respectively. A statistical analysis of the residuals of the least-squares computation shows that within each of the three sets the standard deviations of $g$ and $h$ are just below 0·1, which is of the order of magnitude of the differences between the results of the three sets. A factor that may contribute to the differences between the results of the three sets is a possible small difference in the orientation of the elastogram for the measurement of $2r$. The final values of the errors of $g$ and $h$ are those calculated from the averaging of the results of the three determinations, namely:

$$g = 75{\cdot}2 \pm 0{\cdot}06; \quad h = 41{\cdot}6 \pm 0{\cdot}04 .$$

It follows that:

$$c_{44} = h - c_{33} = 8{\cdot}8 \pm 0{\cdot}08 ,$$
$$c_{55} = g - c_{11} = 8{\cdot}3 \pm 0{\cdot}18 .$$

The larger error in $c_{55}$ derives mainly from the error in $c_{11}(\pm 0{\cdot}12)$. Fortunately it was possible to reduce it in the following way: in some elastograms the outer curve nearly reaches the $Y$ axis; it is possible to ascertain on them the value of $2r$ along the $Y$ axis, with less accuracy than the other measurements, but still with sufficient accuracy to obtain a better value of $c_{55}$. In this way the error in $c_{55}$ was reduced to 0·09. (For instance, $2r_{T_y} = (3{\cdot}53 \pm 0{\cdot}02)$ mm., with $\nu = 4{\cdot}9782$ mHz., $\gamma = 31{\cdot}12$, gives $Q = c_{55} = 8{\cdot}28 \pm 0{\cdot}09$).

Also the stiffness $c$ was calculated. This was done from the values of $Q_T$ in the region between $\varphi = 36°$ and 54°. In this region (around 45°) any possible errors in $c_{44}$ and $c_{55}$ have the least effect on $c$. The value obtained is $28{\cdot}4 \pm 0{\cdot}2$. From the definition of $c$ (7) and the values of $c$, $c_{44}$ and $c_{55}$, it follows: $c_{13} = 19{\cdot}9 \pm 0{\cdot}3$.

Then the '$a_i$' calculation was carried out (equations (24) and (25)). The same experimental data used for the '$gh$' calculation could be used here. It was thought first that, as the relative errors of the $Q_T$ are smaller than those of the $Q_L$ and also because the outer curve is more sensitive to a change in $c_{44}$ and $c_{55}$, it would be better to use the $Q_T$ values only. This was done, and the values obtained for the $a_i$—and hence for the $c_{ij}$—were quite far from the correct ones. This is a consequence of fitting the outer curve only, and neglecting the information contained in the inner curve. The residuals for the outer curve are thus very small and give an illusion of accuracy; but if they are calculated for the inner curve as well, they are quite large. Therefore, this calculation must make use of both $Q_T$ and $Q_L$. Instead of 21 equations there are 42; and if the measurements of $Q_L$ along $Y$ and $Z$ are added ($c_{11}$ and $c_{33}$), the number of linear equations becomes 44 (with the 5 variables, $a_i$).

The solutions, for the same three sets of data used in the '$gh$' calculation, are given in Table 2.

Table 2. *Results of three separate determinations of the values $a_1 \ldots a_5$*

| | (1) | (2) | (3) |
|---|---|---|---|
| $a_1$ | 75·22 | 75·09 | 75·22 |
| $a_2$ | 41·69 | 41·78 | 41·46 |
| $a_3$ | 556·5 | 557·0 | 553·8 |
| $a_4$ | 294·6 | 298·9 | 284·8 |
| $a_5$ | 1454 | 1443 | 1465 |

The values of the $c_{ij}$ follow by means of (24) and (7); they are given in Table 3.

Table 3. *Results of the determinations of the five elastic constants by the '$gh$' and '$a_i$' methods*

| | '$gh$' | | | '$a_i$' | | | Averages | |
|---|---|---|---|---|---|---|---|---|
| $c_{ij}$ | (1) | (2) | (3) | (1) | (2) | (3) | '$gh$' | '$a_i$' |
| $c_{11}$ | — | — | — | 66·9 | 66·8 | 67·0 | 66·9 | 66·9 |
| $c_{33}$ | — | — | — | 32·7 | 32·6 | 32·8 | 32·8 | 32·7 |
| $c_{13}$ | — | — | — | 19·8 | 19·8 | 19·8 | 19·9 | 19·8 |
| $c_{44}$ | 8·8 | 8·8 | 8·7 | 9·0 | 9·1 | 8·7 | 8·8 | 8·9 |
| $c_{55}$ | 8·4 | 8·2 | 8·3 | 8·3 | 8·3 | 8·3 | 8·3 | 8·3 |

In comparing the results of '$gh$' with those of '$a_i$', it should be noticed that the second one has the advantage that it is in principle a more direct approach; but it gives the same weight to all the data. (It is of course possible to assign weights to the different measurements, and introduce them in the calculations; but this was thought not to be necessary, as the '$gh$' method was available.) The '$gh$' method, on the other hand, has the advantage of using directly the accurately determined values of $c_{11}$ and $c_{33}$ and this increases the accuracy of $c_{44}$ and $c_{55}$.

With the values of $c_{ij}$ thus obtained it is possible to calculate the stiffnesses $Q_L$ and $Q_T$ for the same directions in which they have been measured in order to compare the calculated values with the experimental values. In this comparison, more importance should be attached to $Q_T$ (the outer curve), not only because the relative errors in the measurements of $2r_T$ are smaller, but also because the outer curve is more sensitive to variations in $c_{44}$ and $c_{55}$ than the inner curve. Table 4 gives the experimental values of $Q_T$ for each of the 3 sets of measurements (1, 2 and 3), and three calculated sets: (*a*) the elastic constants determined by us with the '$gh$' method; $c_{44}=8{\cdot}8$, $c_{55}=8{\cdot}3$; (*b*) the same, but with $c_{44}=c_{55}=8{\cdot}5$, a mean value between our $c_{44}$ and $c_{55}$; (*c*) the same, but with $c_{44}=c_{55}=8{\cdot}3$, the value obtained for $c_{55}$ which was more directly accessible than $c_{44}$. Should the Voigt theory be applicable, then the experimental values of $Q_T$ would have to conform to tables such as (*b*) or (*c*). It can be seen that column (*a*) fits the experimental values better than the other two.

Table 4. *Experimental and calculated values of $Q_T$*

| | Experimental | | | | Calculated | | |
|---|---|---|---|---|---|---|---|
| $\varphi$ | (1) | (2) | (3) | Average | (*a*) | (*b*) | (*c*) |
| 9 | 8·57 | 8·57 | 8·55 | 8·56 | 8·56 | 8·76 | 8·56 |
| 12 | 8·73 | 8·75 | 8·73 | 8·74 | 8·76 | 8·95 | 8·75 |
| 15 | 9·00 | 9·00 | 8·99 | 9·00 | 9·01 | 9·19 | 8·99 |
| 18 | 9·32 | 9·34 | 9·34 | 9·33 | 9·30 | 9·48 | 9·30 |
| 21 | 9·65 | 9·67 | 9·62 | 9·65 | 9·64 | 9·80 | 9·62 |
| 24 | 9·98 | 10·02 | 9·98 | 9·99 | 10·00 | 10·16 | 10·00 |
| 27 | 10·37 | 10·35 | 10·35 | 10·36 | 10·39 | 10·53 | 10·39 |
| 30 | 10·74 | 10·69 | 10·76 | 10·73 | 10·79 | 10·92 | 10·78 |
| 33 | 11·18 | 11·15 | 11·21 | 11·18 | 11·20 | 11·31 | 11·19 |
| 36 | 11·61 | 11·56 | 11·54 | 11·57 | 11·58 | 11·69 | 11·57 |
| 39 | 12·02 | 12·00 | 11·98 | 12·00 | 11·96 | 12·04 | 11·92 |
| 42 | 12·35 | 12·35 | 12·26 | 12·32 | 12·30 | 12·36 | 12·24 |
| 45 | 12·60 | 12·62 | 12·60 | 12·61 | 12·57 | 12·61 | 12·51 |
| 48 | 12·77 | 12·74 | 12·74 | 12·75 | 12·78 | 12·80 | 12·70 |
| 51 | 12·86 | 12·88 | 12·86 | 12·87 | 12·90 | 12·89 | 12·79 |
| 54 | 12·86 | 12·85 | 12·93 | 12·88 | 12·91 | 12·86 | 12·76 |
| 57 | 12·83 | 12·80 | 12·85 | 12·83 | 12·81 | 12·73 | 12·63 |
| 60 | 12·62 | 12·57 | 12·55 | 12·58 | 12·59 | 12·48 | 12·36 |
| 63 | 12·29 | 12·26 | 12·29 | 12·28 | 12·25 | 12·12 | 12·00 |
| 66 | 11·89 | 11·87 | 11·87 | 11·88 | 11·83 | 11·66 | 11·54 |
| 69 | 11·34 | 11·37 | 11·37 | 11·36 | 11·33 | 11·13 | 10·99 |

The $Q_T$ have also been calculated with the $c_{ij}$ obtained from the $a_i$ computation; these differed from the experimental values a little more than the calculated values of column (*a*), thus proving that the results of our '$gh$' calculation fit the outer curve of the elastograms better than those of the '$a_i$' calculation. Our final results for the adiabatic elastic constants are, thus:

$$\begin{aligned} c_{11} &= (66{\cdot}9 \pm 0{\cdot}12).10^{10} \text{ dyne cm.}^{-2} \\ c_{33} &= 32{\cdot}8 \pm 0{\cdot}04 \\ c_{13} &= 19{\cdot}9 \pm 0{\cdot}3 \\ c_{44} &= 8{\cdot}8 \pm 0{\cdot}08 \\ c_{55} &= 8{\cdot}3 \pm 0{\cdot}09 \end{aligned}$$

whence it follows that

$$\begin{aligned} c_{44}-c_{55} &= 0{\cdot}5 \pm 0{\cdot}17 \\ (c_{44}-c_{55})/c_{44} &= 6\% \ (\pm 2\%) \ . \end{aligned}$$

The effect on the results of misorientation of the specimen, for measurements along $Y$ and $Z$, may be illustrated as follows. A deviation of 3° from their true directions within the $YZ$ plane of the $Y$ and $Z$ axes, would change the values of $c_{11}$, $c_{33}$, $c_{44}$ and $c_{55}$ from 66·90, 32·80, 8·80, 8·30 to 66·78, 32·82, 8·87, 8·33; and deviations of 3° in any other direction would cause still smaller changes. So, even a deviation of 1° would cause errors smaller than our quoted errors and negligible compared with $c_{44}-c_{55}$. As has been mentioned in Section 3, all the errors in orientation amount to no more than a few minutes of arc.

Finally, we wish to stress that the errors quoted are for the *relative* (not *absolute*) values of the $c_{ij}$.

The difference of 6% (±2%) between $c_{44}$ and $c_{55}$ is in contradiction with the classical theory of crystal elasticity but fits into the more general theory put forward by Laval. The amount of this difference is much too large to be accounted for by the coupling between elastic and piezoelectric properties.

In a recent paper Joel & Wooster (1958*b*) reported that a difference of 8% (±1%) between $c_{44}$ and $c_{55}$ could be detected on Zwicker's (1946) elastogram of *ADP*. The estimate of the error, ±1%, was probably too optimistic as we did not at that time consider the effect of the errors in $c_{11}$ and $c_{33}$ on the outer curve.

We wish to acknowledge the kind cooperation of Mr C. W. Oatley, in designing the oscillator used in this work, and in arranging for its construction at the Engineering Laboratory of Cambridge University, and also the Admiralty Research Station, for its generosity in supplying the excellent single crystal of *ADP* which

was used in the preparation of our specimens. We are much indebted to Mr E. G. Menage (149 Howard Road, Woodside, London S.E. 25), for his successful grinding and polishing of the specimens and to the Technical Department of Ilford, Ltd., for supplying technical data on their films *HP*3 and *HPS*. We wish to thank the Mathematical Laboratory of Cambridge University for the use of the electronic computer EDSAC without which the large number of computations would have been impossible.

One of us (N. J.) has great pleasure in expressing his gratitude to Prof. N. F. Mott, F.R.S. and Dr W. H. Taylor, for providing the facilities of the Cavendish Laboratory and for their encouragement; Mr C. W. Oatley, for his helpful advice; Prof. J. Laval and Dr Y. LeCorre, for stimulating discussions during a visit to their Laboratory in Paris; the British Council, for a research scholarship while on leave of absence from the University of Santiago-Chile.

### References

BERGMANN, L. (1954). *Der Ultraschall*, 6th ed. Stuttgart: Hirzel.

BORN, M. & HUANG, K. (1954). *Dynamical Theory of Crystal Lattices*. Oxford: Clarendon Press.

FUES, E. & LUDLOFF, H. (1935). *S. B. Berliner Akad. Wiss. Phys. Math.* **14**, 225.

HAUSSÜHL, S. (1957). *Fortschr. Min.* **35**, 4.

HUGHES, W. & TAYLOR, C. A. (1953). *J. Sci. Instrum.* **30**, 105.

JOEL, N. & WOOSTER, W. A. (1957). *Nature, Lond.* **180**, 430.

JOEL, N. & WOOSTER, W. A. (1958*a*). *Nature, Lond.* **182**, 1078.

JOEL, N. & WOOSTER, W. A. (1958*b*). *Acta Cryst.* **11**, 575.

JONA, F. (1950). *Helv. Phys. Acta*, **23**, 795.

LAVAL, J. (1951). *C. R. Acad. Sci., Paris*, **232**, 1947.

LAVAL, J. (1952). *L'état Solide*. Rapports et Discussions, Congrès Solvay 1951. Bruxelles: Stoops.

LAVAL, J. (1957). *J. Phys. Radium*, **18**, 247, 289, 369.

LECORRE, Y. (1954). *Bull. Soc. franç. Minér. Crist.* **77**, 1363.

NOMOTO, O. (1943). *Proc. Phys. Math. Soc., Jap.* **25**, 240.

SPANGENBERG, K. & HAUSSÜHL, S. (1957). *Z. Kristallogr.* **109**, 422.

TOPPING, J. (1955). *Errors of Observation and their Treatment*. London: The Institute of Physics.

ZUBOV, V. G. & FIRSOVA, M. M. (1956). *Kristallographia*, **1**, 546.

ZWICKER, B. (1946). *Helv. Phys. Acta*, **19**, 523.

*Acta Cryst.* (1960). **13**, 525

# The Crystal and Molecular Structure of *dl*-Alphaprodine Hydrochloride

BY G. KARTHA,* F. R. AHMED AND W. H. BARNES

*Pure Physics Division, National Research Council, Ottawa, Canada*

(*Received* 30 *October* 1959)

The structure of the hydrochloride of *dl*-alphaprodine (*dl*-α-1:3-dimethyl-4-phenyl-4-propionoxy piperidine) has been determined by the isomorphous-replacement method with the aid of data for the hydrobromide. Zero-level normal, and first-level generalized, projections along the three axes have been employed. The structure has been refined by three-dimensional Fourier and differential syntheses. The stereochemical configuration found for the alphaprodine molecule agrees with that of one of four possible isomers and confirms that proposed by Beckett and co-workers on conformational and other grounds. The piperidine ring has the chair form with the phenyl ring equatorial and the propionoxy chain axial; the methyl group on C(3) is *trans* to the phenyl ring on C(4).

## Introduction

Ziering & Lee (1947) were the first to prepare *dl*-1:3-dimethyl-4-phenyl-4-propionoxy piperidine, $C_{16}H_{23}NO_2$, and to show that it can be obtained in two diastereoisomeric (α and β) forms which have since received the common names, alphaprodine (Nisentil$^R$) and betaprodine. Alphaprodine hydrochloride has a higher melting point and lower analgesic potency than the corresponding salt of the beta isomer.

Four *cis–trans* configurations of the molecule of 1:3-dimethyl-4-phenyl-4-propionoxy piperidine are possible according to the relative positions of H and $CH_3$ attached to C(3) and of $OCOC_2H_5$ and $C_6H_5$ attached to C(4) of the piperidine ring. Assuming that this ring has the chair form, the several possible isomers are illustrated in Fig. 1, where Ph = phenyl ($C_6H_5$), Pr = propionoxy ($OCOC_2H_5$), Me = methyl ($CH_3$), *a* = axial to the piperidine ring, *e* = equatorial to the piperidine ring.

Some important relationships are summarized in Table 1, from which it is apparent that the *cis* or *trans* designation of the members of a single pair of prodine

* National Research Council Postdoctorate Fellow, now in the Biophysics Department, Rosewell Park Memorial Institute Buffalo, N. Y.